Detection of Surface Orientation and Motion from Texture by a Stereological Technique*

Ken-ichi Kanatani
Department of Computer Science, Gunma University, Kiryu, Gunma 376, Japan

Recommended by H.H. Nagel

ABSTRACT
A new approach is given to detect the surface orientation and motion from the texture on the surface by making use of a mathematical principle called 'stereology'. Information about the surface orientation is contained in 'features' computed by scanning the image by parallel lines and counting the number of intersections with the curves of the texture. A synthetic example is given to illustrate the technique. This scheme can also detect surface motions relative to the viewer by computing features of its texture at one time and a short time later. The motion is specified by explicit formulae of the computed features.

1. Introduction

The detection of surface orientation from texture is one of the most important topics (or 'modules') of computer vision (e.g., [1]). One approach is to compute the 'gradient' obtained by differentiating the apparent density on the assumption that the true surface texture is 'spatially homogeneous'. This approach was initiated by Gibson [2, 3], and there have been several works on this line. For instance, Bajcsy and Lieberman [4] tried a heuristic use of the two-dimensional Fourier spectrum to detect the gradient. This approach is also viewed in terms of actual human perception (e.g., see [5]). On the other hand, Witkin [6] recently presented a statistical approach without assuming spatial homogeneity. Instead, he assumed 'directional isotropy', i.e., the assumption that the peripheral contours of the figures in the true texture have line segments of all possible orientations and that their distribution is uniform over all orientations.

* Part of this work was done under the support of Saneyoshi Scholarship Foundation.

Artificial Intelligence **23** (1984) 213–237
0004-3702/84/$3.00

This is based on the following observation. Motivated to simulate human perception, he confines the surfaces under consideration to only those whose orientations could be easily perceived from the texture by human eye. If the true texture is not isotropic and has a preferred orientation, it 'mimics' a projected image and thus makes it impossible to detect the true orientation even by human eye. His procedure is summarized as follows. Suppose a given texture image is transformed into lines and curves, say, by convolution of $\nabla^2 G$ and application of the 'zero-crossing' [1]. Then:

(i) dissect all the curves in the texture into small line segments by tracing them;

(ii) classify the line segments according to their orientations and make a histogram;

(iii) Assume the true angles of the 'slant' and the 'tilt' and compute the 'statistical likelihood' that the observed histogram is obtained from a uniform population distribution;

(iv) compute the likelihood for all possible angle pairs of the slant and the tilt and search the two-dimensional domain for the pair that maximizes the likelihood.

All (i)–(iv) are time-consuming processes, and, as is well known, the histogram is sensitively affected by the choice of the class interval. It must be neither too large nor too small. In this paper, we will show that none of them is necessary at all, if we are to adopt the same statistical assumption and to pursue the same objective. The basic principle is stated in general terms as follows. Suppose that the object is described by a model involving several free parameters and that our purpose is to determine the values of these parameters from its projected image. Given an image as input data, we first extract a small number of values characteristic of the image, which we call 'features'. Then, we study mathematical relationships between these features and the object parameters and derive a set of algebraic equations involving them. The rest of the job is to solve them either analytically or numerically. This is a familiar approach in pattern recognition problems. (See [7, 8] for a general framework.) The most crucial point in this approach is a good choice of features with which enough mathematical vigor is associated.

Our method is based on a mathematical principle called 'integral geometry' or 'stereology' [9–18]. Application of this branch of mathematics to extract information about deformation of a given pattern was fully studied by Kanatani [19]. In this paper, we show that a two-dimensional version of his theory serves the above-mentioned purpose. The features we use are a pair of second Fourier harmonics of the data of intersections between the texture and parallel scanning lines. Our technique is illustrated by a synthetic example. Moreover, we show that the same technique can be used to detect from the projected texture alone the motion of a surface which rotates relative to the viewer. In this case, even the directional isotropy need not be assumed. This is a good example that

an abstract mathematical study gives rise to effective computer algorithms to problems which otherwise require long and tedious processes and furthermore leads to discoveries of completely new applications. This also unveils the fact that seemingly unrelated branches of science are often closely interwoven in terms of mathematics.

2. Two-dimensional Buffon Transform

In the following, we use polar coordinates to describe orientations, assuming a fixed reference xy-coordinate system. Suppose curves are distributed on the plane. The 'distribution density' $f(\theta)$ is defined as follows. Dissect the curves into infinitesimal line elements of length $\mathrm{d}l$. The orientation of each line element is specified by the angle θ from the reference x-axis. Since there are two possibilities, i.e., θ and $\theta + \pi$, choose either of them randomly with probability $\frac{1}{2}$. Let $f(\theta)$ be defined in such a way that $f(\theta)\,\mathrm{d}\theta$ is the total length per unit area of those line elements whose orientations are between θ and $\theta + \mathrm{d}\theta$. Obviously $f(\theta)$ is 'symmetric', i.e., $f(\theta) = f(\theta + \pi)$, and $\int_0^{2\pi} f(\theta)\,\mathrm{d}\theta$ is the total length of the curves per unit area. (Caution: The dissection of the curves and the random selection of orientation described above are merely mathematical conceptions and are not performed actually. We could have alternatively defined $f(\theta)$ for $0 \leqq \theta < \pi$, copying it for $\pi \leqq \theta < 2\pi$ and dividing it by 2.)

Place a line of orientation ϕ randomly on the plane and consider the expected number of intersections with the curves. The probability that a line element of orientation between θ and $\theta + \mathrm{d}\theta$ intersects the line is equal to the probability that the center of the line element falls within a strip of width $|\sin(\phi - \theta)|\,\mathrm{d}l$ along the line (Fig. 1). Since there are $f(\theta)\,\mathrm{d}\theta/\mathrm{d}l$ such line elements per unit area, that probability is equal to $|\sin(\phi - \theta)|f(\theta)\,\mathrm{d}\theta$ per unit length of the probe line. The probability of finding an intersection is equal to

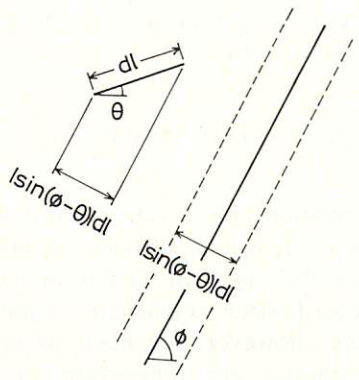

FIG. 1. A line element intersects the probe line when its center falls within a strip of width $|\sin(\phi - \theta)|\,\mathrm{d}l$ along the probe line.

the expected number of intersections, so that the expected number of intersections per unit length is given by

$$N(\phi) = \int_0^{2\pi} |\sin(\phi - \theta)| f(\theta)\, \mathrm{d}\theta\,. \tag{1}$$

This derivation is rigorous because we are not concerned with the 'spatial correlations'. This relation has long been well known. Kanatani [19] called it the 'Buffon transform' after the pioneer more than two centuries ago [20]. Equation (1) expresses the expected value, but if we repeat the 'line dropping' independently a large number of times it is interpreted as the average over those trials due to the 'law of large numbers'. It is in this sense that (1) has a realistic meaning.

3. Inverse Buffon Transform

If we have an inversion formula of (1), we can determine the distribution density $f(\theta)$ from the data of intersection counting. This is done by expanding $N(\phi)$ into Fourier series

$$N(\phi) = \frac{C}{2\pi}\left[1 + \sum_{n=2}^{\infty}{}' (A_n \cos n\phi + B_n \sin n\phi)\right], \tag{2}$$

$$C = \int_0^{2\pi} N(\phi)\, \mathrm{d}\phi\,, \tag{3}$$

$$A_n = \frac{2}{C}\int_0^{2\pi} N(\phi)\cos n\phi\, \mathrm{d}\phi\,, \qquad B_n = \frac{2}{C}\int_0^{2\pi} N(\phi)\sin n\phi\, \mathrm{d}\phi\,, \tag{4}$$

where $\sum'$ designates summation of even-indexed terms only. (Terms of odd n do not appear because $N(\phi)$ is 'symmetric', i.e., $N(\phi + \pi) = N(\phi)$.) Then, the distribution density $f(\theta)$ is given by

$$f(\theta) = \frac{\frac{1}{4}C}{2\pi}\left[1 - \sum_{n=2}^{\infty}{}' (n^2 - 1)(A_n \cos n\theta + B_n \sin n\theta)\right]. \tag{5}$$

(See Appendix A for derivation.) Here, one might think that application of the Fast Fourier Transform (FFT) would provide an efficient algorithm for this conversion. But that is not the case. The FFT is an algorithm to compute all of the prescribed N (discrete) Fourier coefficients simultaneously by an effective scheme (e.g., [21]). Here, however, we need to compute only a few low harmonics, and high harmonics are unnecessary or even hazardous. This is because statistical fluctuations are inevitable for observed data and the inverse Buffon transform drastically amplifies high harmonics. Hence, the observed $N(\phi)$ must be properly 'smoothed' beforehand, say, by applying an appropriate

low-pass filter. But application of a low-pass filter means nothing but neglecting high harmonics of the Fourier expansion.

To be specific, only A_2 and B_2 are necessary to detect the orientation of the surface, as will be shown later. The idea behind this is as follows. As is familiar in differential geometry, any smooth deformation of the space is characterized by a tensor field of second rank. On the other hand, A_2 and B_2 form, if properly arranged, a two-dimensional tensor of second rank (cf. [22]). Hence, these two tensors of the same rank must be related by a tensor equation invariant to coordinate translations and rotations.

As an example, consider the pattern of Fig. 2, which is obtained after distorting an initially isotropic random pattern drawn by random numbers. The count of intersections are shown by the circular diagram of Fig. 3, where the scale is chosen so that the average value becomes $1/2\pi$. We used equally spaced parallel lines whose spacing is 1/22 of one side of the square frame for orientations $\pi k/N$, $k = 0, 1, \ldots, N-1$, and we chose N to be 16, i.e., at 11.25° intervals. Let N_k be the number of intersections per unit length at $\phi = \pi k/N$. In view of (3) and (4), the coefficients C, A_2 and B_2 are computed respectively by

$$C = 2\pi \sum_{k=0}^{N-1} N_k \Big/ N, \tag{6}$$

$$A_2 = 2 \sum_{k=0}^{N-1} N_k \cos(2\pi k/N) \Big/ \sum_{k=0}^{N-1} N_k,$$

$$B_2 = 2 \sum_{k=0}^{N-1} N_k \sin(2\pi k/N) \Big/ \sum_{k=0}^{N-1} N_k . \tag{7}$$

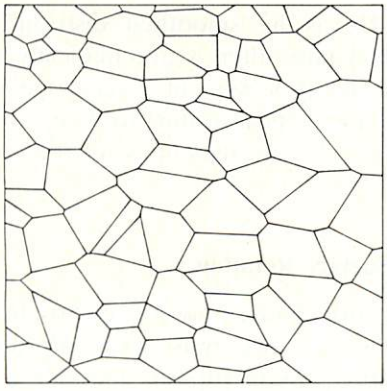

FIG. 2. An artificial pattern obtained after distorting an initially isotropic random pattern drawn by random numbers.

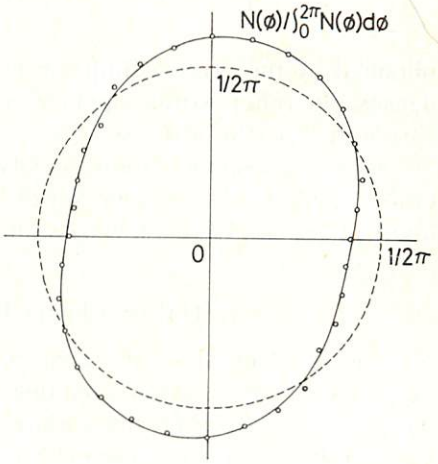

FIG. 3. Normalized data of intersection counting on Fig. 2 and the curve fitted up to the second harmonics.

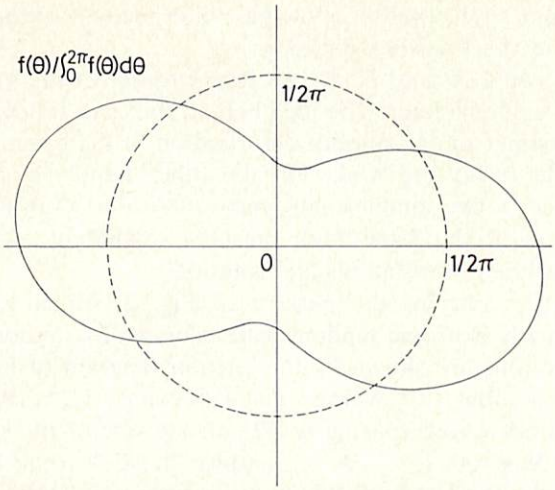

FIG. 4. The distribution density of line segments of Fig. 2 obtained by the inverse Buffon transform of the curve of Fig. 3.

(Note the angle $2\pi k/N$. We are computing 'second' Fourier coefficients. First coefficients are zero by definition.) The solid curve in Fig. 3 is $N(\phi)/\int_0^{2\pi} N(\phi)\,d\phi = 1 + A_2 \cos 2\phi + B_2 \sin 2\phi$ obtained by neglecting higher harmonics. In this case we obtain $A_2 = -0.172$ and $B_2 = 0.068$. Fig. 4 plots the normalized distribution density

$$f(\theta) \Big/ \int_0^{2\pi} f(\theta)\,d\theta = 1 - 3(A_2 \cos 2\theta + B_2 \sin 2\theta)$$

obtained by the inverse Buffon transform. This is the 'smoothed' distribution density. In other words, application of a low-pass filter is automatically incorporated in this process. This saves all the processes of tracing curves, executing their segmentation, classifying the segments according to their orientations, making a histogram, which is very sensitive to the choice of the class interval, and applying a low-pass filter.

4. Texture Change Due to Surface Rotation

Now, we give an algorithm to calculate the surface orientation explicitly from the data of intersection counting. To this end, we must first introduce parameters to describe the surface orientation. As in [6], we consider only 'orthographic' distortions and neglect 'projective' distortions. We define the 'slant' and the 'tilt' as follows. Consider a plane with a texture on it, and take an xy-coordinate system on it. Put a line passing the origin on it, and let τ be

its angle made from the x-axis. Rotate the plane around the line by angle σ (in whichever sense) and project the rotated plane orthographically onto the original plane. As is seen easily, this process distorts the texture in such a way that it shrinks by $\cos\sigma$ in the direction normal to the rotation axis but not in the direction of the rotation axis. We call σ the 'slant' and τ the 'tilt'. Our task is, therefore, to invert this process and recover the original texture only by looking at the distorted texture.

As is easily confirmed, the distortion described above is a two-dimensional linear transformation written as

$$\boldsymbol{r}' = \boldsymbol{T}\boldsymbol{r}, \tag{8}$$

$$\boldsymbol{T} = \begin{bmatrix} 1-(1-\cos\sigma)\sin^2\tau & (1-\cos\sigma)\sin\tau\cos\tau \\ (1-\cos\sigma)\sin\tau\cos\tau & 1-(1-\cos\sigma)\cos^2\tau \end{bmatrix}. \tag{9}$$

(See Appendix B for derivation.) A unit vector $\boldsymbol{n} = (\cos\theta, \sin\theta)^{\mathrm{T}}$, T standing for transpose, is transformed to $\boldsymbol{Tn}$, and it is no longer a unit vector. Its length is

$$L(\theta) = \sqrt{\boldsymbol{n}^{\mathrm{T}}\boldsymbol{T}^{\mathrm{T}}\boldsymbol{T}\boldsymbol{n}}\,. \tag{10}$$

Hence, the unit vector $\boldsymbol{n}' = (\cos\theta', \sin\theta')^{\mathrm{T}}$ of the transformed direction is given by

$$\boldsymbol{n}' = \boldsymbol{T}\boldsymbol{n}/L(\theta)\,. \tag{11}$$

This can be viewed as a 'map' of a unit circle onto itself. Its 'Jacobian' $\mathrm{d}\theta'/\mathrm{d}\theta$ is given by

$$\mathrm{d}\theta'/\mathrm{d}\theta = \det\boldsymbol{T}/L(\theta)^2\,. \tag{12}$$

(See Appendix C for derivation.) If $f(\theta)$ is the original distribution density of line segments, the distribution density after transformation (9) is then given by

$$f(\theta') = \frac{L(\theta)}{\det\boldsymbol{T}} f(\theta) \Big/ \frac{\mathrm{d}\theta'}{\mathrm{d}\theta}\,. \tag{13}$$

Here, $\det\boldsymbol{T}$ appears because $f(\theta)$ is defined per unit area. Thus, the transformation of the distribution density has a very complicated form. The 'trick' we use here is that we consider only a 'small slant'. By the Taylor expansion, we have

$$\cos\sigma = 1 - \tfrac{1}{2}\sigma^2 + \tfrac{1}{24}\sigma^4 - \cdots\,.$$

If only those terms up to σ^2 are retained, which is a fairly good approximation for $-\frac{1}{4}\pi < \sigma < \frac{1}{4}\pi$, equations (10)–(13) and det $\boldsymbol{T}$, respectively, become as follows:

$$L(\theta) = 1 - \tfrac{1}{4}\sigma^2(1 - \cos 2(\theta - \tau)) + O(\sigma^4), \tag{14}$$

$$\begin{bmatrix}\cos\theta' \\ \sin\theta'\end{bmatrix} = \begin{bmatrix}\cos\theta \\ \sin\theta\end{bmatrix} + \tfrac{1}{4}\sigma^2\left(\begin{bmatrix}\cos(2\tau - \theta) \\ \sin(2\tau - \theta)\end{bmatrix} - \cos 2(\theta - \tau)\begin{bmatrix}\cos\theta \\ \sin\theta\end{bmatrix}\right) + O(\sigma^4), \tag{15}$$

$$\frac{d\theta'}{d\theta} = 1 - \tfrac{1}{2}\sigma^2 \cos 2(\theta - \tau) + O(\sigma^4), \tag{16}$$

$$\det \boldsymbol{T} = 1 - \tfrac{1}{2}\sigma^2 + O(\sigma^4). \tag{17}$$

Here, $O(\sigma^4)$ designates terms of σ whose orders are equal to or higher than 4. (See Appendix D for derivation.)

Now, suppose the initial distribution density has the form

$$f(\theta) = \frac{c}{2\pi}[1 + a_2 \cos 2\theta + b_2 \sin 2\theta]. \tag{18}$$

the distribution density after transformation (9) becomes

$$f(\theta') = \frac{c'}{2\pi}[1 + a_2' \cos 2\theta' + b_2' \sin 2\theta' + a_4' \cos 4\theta' + b_4' \sin 4\theta'] + O(\sigma^4), \tag{19}$$

$$c' = c[1 + \tfrac{1}{4}\sigma^2(1 + \tfrac{1}{2}(a_2 \cos 2\tau + b_2 \sin 2\tau))], \tag{20}$$

$$a_2' = a_2 + \tfrac{1}{4}\sigma^2[3 \cos 2\tau - \tfrac{1}{2}a_2(a_2 \cos 2\tau + b_2 \sin 2\tau)], \tag{21}$$

$$b_2' = b_2 + \tfrac{1}{4}\sigma^2[3 \sin 2\tau - \tfrac{1}{2}b_2(a_2 \cos 2\tau + b_2 \sin 2\tau)], \tag{22}$$

$$\begin{aligned} a_4' &= \tfrac{5}{2}\sigma^2(a_2 \cos 2\tau - b_2 \sin 2\tau), \\ b_4' &= \tfrac{5}{2}\sigma^2(a_2 \sin 2\tau + b_2 \cos 2\tau). \end{aligned} \tag{23}$$

(See Appendix E for derivation.) In particular, if the initial distribution density is 'isotropic', i.e., $f(\theta) = c/2\pi$, the distribution density after transformation (9) becomes

$$f(\theta') = \frac{c}{2\pi}(1 + \tfrac{1}{4}\sigma^2)[1 + \tfrac{3}{4}\sigma^2(\cos 2\tau \cos 2\theta' + \sin 2\tau \sin 2\theta')] + O(\sigma^4).$$

Hence, its Buffon transform becomes

$$N(\phi') = \frac{4c}{2\pi}(1+\tfrac{1}{4}\sigma^2) \times [1-\tfrac{1}{4}\sigma^2(\cos 2\tau \cos 2\phi' + \sin 2\tau \sin 2\phi')] + O(\sigma^4)\,.$$

It follows that if we count intersections and express the data in the form

$$N(\phi') \sim \frac{C}{2\pi}[1 + A_2 \cos 2\phi' + B_2 \sin 2\phi']\,,$$

by (6) and (7), we get as a first approximation

$$C = 4c(1+\tfrac{1}{4}\sigma^2)\,, \tag{24}$$

$$A_2 = -\tfrac{1}{4}\sigma^2 \cos 2\tau, \qquad B_2 = -\tfrac{1}{4}\sigma^2 \sin 2\tau\,. \tag{25}$$

Hence, the slant σ and the tilt τ are given by

$$\sigma = \pm 2((A_2)^2 + (B_2)^2)^{1/4}\,, \tag{26}$$

$$\tau = \begin{cases} \tfrac{1}{2}\tan^{-1}\dfrac{B_2}{A_2}, & A_2 < 0\,, \\ \tfrac{1}{2}\pi + \tfrac{1}{2}\tan^{-1}\dfrac{B_2}{A_2}, & A_2 > 0\,. \end{cases} \tag{27}$$

where $\tan^{-1}$ designates the principal value, $-\frac{1}{2}\pi < \tan^{-1} x < \frac{1}{2}\pi$. (If $A_2 = 0$, then $\tau = -\frac{1}{4}\pi$ for $B_2 > 0$ and $\tau = \frac{1}{4}\pi$ for $B_2 < 0$. If $A_2 = B_2 = 0$, σ is not defined because there is no slant.) The whole procedure is summarized as follows.

(i) Scan the plane by parallel lines along orientations $\phi = \pi k/N$, for $k = 0, 1, \ldots, N-1$, and let N_k be the number of intersections per unit length of the scanning lines.

(ii) Compute A_2 and B_2 by (6) and (7).

(iii) The slant σ and the tilt τ are given by (26) and (27).

As for the example of Fig. 2, the slant σ and the tilt τ are readily available, since A_2 and B_2 are already obtained. We obtain $\sigma = \pm 49.3°$ and $\tau = -10.8°$. (Note that the tilt is given as the angle of the 'minor symmetric axis' of Fig. 3 or the 'major symmetric axis' of Fig. 4.)

This demonstrates how simple our procedure is. In fact, no histogram or maximization search is necessary. The above A_2 and B_2 are the 'features' characterizing information about the orientation of the surface. Once they are obtained, explicit arithmetic computations determine the surface orientation.

Of course, (26) and (27) give only a first approximation, and if the slant σ is large, our solution might be a poor approximation. If that is the case, however, we can still use the solution as a 'first guess' and recover the original texture, i.e., extending the texture $1/\cos\sigma$ times along the direction $(-\sin\tau, \cos\tau)^T$. Then, perform (i), (ii) and (iii) again and make a small correction. In this case, the slant must surely be small. This successive correction can be made as often as is desired.

5. Determination of Surface Motion

In the previous section the assumption of 'directional isotropy' played a crucial role, as was pointed out by Witkin [6]. If the texture is anisotropic, the scheme described there is doomed to fail. On the other hand, textures of artificial or man-made objects usually have systematic structures far from isotropic. That is why Witkin [6] proclaimed that he would avoid 'artifacts'. But is there any way to exploit this strong bias of man-made texture? Equations (18)–(23) suggest that, if we have a 'prior knowledge' of the true texture, the same process can apply to determine the surface orientation. This consideration leads to the idea of determining the 'relative orientation'. Suppose we look at a surface orthographically at a certain instant, and suppose the surface is rotating around an unknown axis with an unknown angular velocity (or equivalently the viewer or the viewing apparatus is moving). Then, a short time later, we look at another image slightly distorted compared with that a moment ago. According to (18)–(23), we can estimate the relative orientation and thus know the rotation axis and the angular velocity.

Determination of three-dimensional motion from a projected two-dimensional motion is one of the important problems in computer vision [1]. Usually, the 'correspondence', i.e., which point has moved to which point, is sought first. After obtaining the velocity field or the 'optical flow', the three-dimensional motion is analyzed (e.g., [23, 24]). Here, however, there is no need of correspondence detection, which is usually a time-consuming process. This is because all relevant information is contained in the features A_2 and B_2.

Suppose the initial distribution is approximated by the form of equation (18). Compute A_2 and B_2 of the initial texture by (7). Similarly, compute A_2' and B_2' of the texture a short time later. Then, the relative slant σ and the relative tilt τ are determined as follows (see Appendix F for derivation).

$$A = (\tfrac{2}{3} - (B_2)^2)(A_2' - A_2) + A_2B_2(B_2' - B_2)\,, \tag{28}$$

$$B = A_2B_2(A_2' - A_2) + (\tfrac{2}{3} - (A_2)^2)(B_2' - B_2)\,, \tag{29}$$

$$\sigma = \pm 2(A^2 + B^2)^{1/4} / |\tfrac{2}{3} - (A_2)^2 - (B_2)^2|^{1/2}\,, \tag{30}$$

$$\tau = \begin{cases} \frac{1}{2}\tan^{-1}\dfrac{B}{A}, & A<0, \\ \frac{1}{2}\pi + \frac{1}{2}\tan^{-1}\dfrac{B}{A}, & A>0. \end{cases} \tag{31}$$

(if $A=0$, the convention in the previous section applies.) For example, consider the texture pattern of Fig. 5(a). Fig. 5(b) is the same texture except that it is rotated with slant 30° and tilt 45°. Fig. 6 shows the normalized data of intersection counting and the curves fitted up to the second harmonics. Here, again we used parallel lines whose spacing is 1/22 of one side of the square frame but this time scanned for 18 different orientations at 10° intervals. Since both of the textures consist only of line segments of 6 different orientations, the corresponding distribution densities have fairly large high harmonics, especially those of the sixth, as can be seen from Fig. 6. Thus, characterizing the textures only by second harmonics might seem a poor approximation. However, if we apply (28)–(31), we obtain $\sigma = \pm 32.2°$ and $\tau = 45.7°$, a remarkable precision in view of the crude approximation. So far, no 'spatial homogeneity' has been assumed, though our examples happened to be spatially homogeneous.

In the above, we assumed that there is no 'in-plane rotation', i.e., rotation around an axis perpendicular to the surface. However, this in-plane rotation can also be included. In this case, the parameters to be determined are the slant σ, the tilt τ and the in-plane rotation Ω. These three parameters are determined if the three features C, A_2 and B_2 are to be used. However, extra

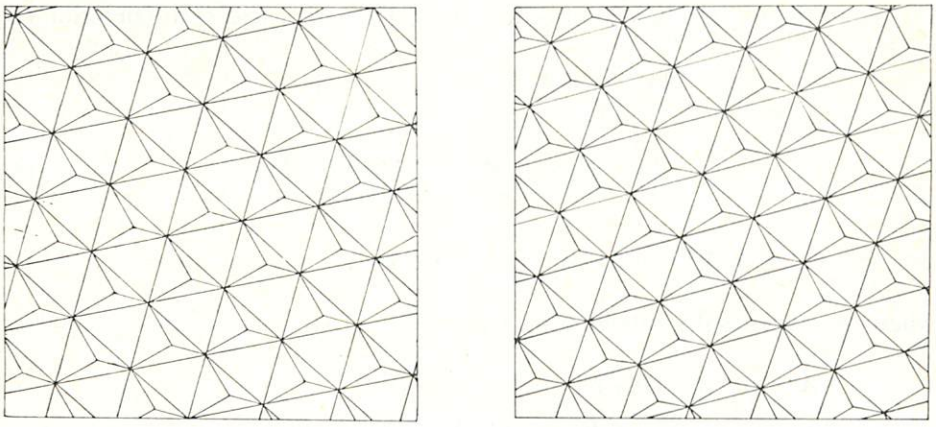

(a) (b)

FIG. 5. (a) An artificial periodic texture pattern. (b) The orthographic projection of the pattern (a) after being inclined with slant 30° and tilt 45°.

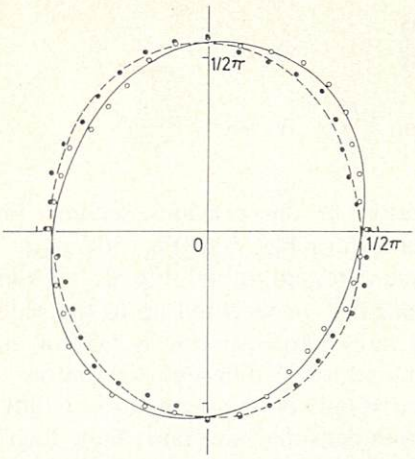

FIG. 6. Normalized data of intersection counting on Fig. 5, circles for (a) and black dots for (b), and their corresponding curves fitted up to the second harmonics, solid curve for (a) and dashed curve for (b).

care must be taken. First, the texture must be spatially homogeneous, because we use C which characterizes the length per unit area. (But actually this limitation is not essential and can be avoided if we remove $\det \boldsymbol{T}$ from (13) and formulating the rest similarly.) Second, which is more crucial, the in-plane rotation Ω must be small compared with the slant σ and must be of order $O(\sigma^2)$. This is understood easily if we note the fact that, if the surface is slanted by σ, the distortion of the projected image is of order $O(\sigma^2)$ while, if the in-plane rotation is Ω, its effect is of order $O(\Omega)$. Since we are dealing with a linearized theory, Ω must be of order $O(\sigma^2)$. Then, σ, τ and Ω are determined by

$$\sigma = \pm 2\left(\frac{C'}{C} - \frac{\|\boldsymbol{A}\|^2 - (\boldsymbol{A}, \boldsymbol{A}')}{\|\boldsymbol{A}\|^2 - \frac{2}{3}} - 1\right)^{1/2}, \tag{32}$$

$$\tau = \tau_0 + \tfrac{1}{2}\cos^{-1}\left[2 \Big/ 3\|\boldsymbol{A}\|\left(1 - \frac{(C'/C - 1)(\|\boldsymbol{A}\|^2 - \frac{2}{3})}{\|\boldsymbol{A}\|^2 - (\boldsymbol{A}, \boldsymbol{A}')}\right)\right], \tag{33}$$

$$\Omega = [[\boldsymbol{A}, \boldsymbol{A}'] + \tfrac{1}{4}\sigma^2\|\boldsymbol{A}\| \sin 2(\tau - \tau_0)]/2\|\boldsymbol{A}\|^2, \tag{34}$$

where we have used symbolic notations

$$\|\boldsymbol{A}\| = ((A_2)^2 + (B_2)^2)^{1/2}, \tag{35}$$

$$(\boldsymbol{A}, \boldsymbol{A}') = A_2A_2' + B_2B_2', \qquad [\boldsymbol{A}, \boldsymbol{A}'] = A_2B_2' - B_2A_2', \tag{36}$$

and τ_0 is the angle defined by

$$\cos 2\tau_0 = A_2/\|\boldsymbol{A}\|, \qquad \sin 2\tau_0 = B_2/\|\boldsymbol{A}\|.$$

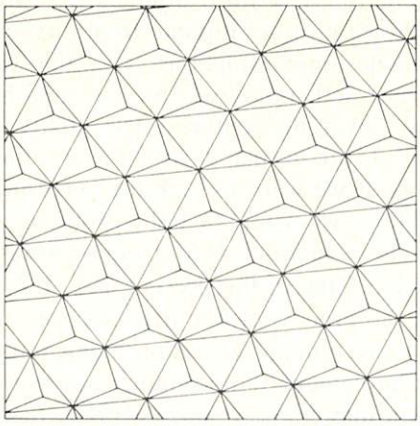

FIG. 7. The pattern of Fig. 5(b) rotated clockwise by 10°.

(See Appendix G for derivation.) The solution is not unique due to the multiple-valuedness of $\cos^{-1}$. In fact, (32)–(34) determine two sets of solutions, and the one with smaller absolute value of Ω must be chosen. For example, consider Fig. 7. This pattern is the same as that of Fig. 5(b) except that it is rotated clockwise by 10°. We obtain $\sigma = \pm 32.9°$, $\tau = 37.7°$ and $\Omega = -10.4°$. The slant σ and in-plane rotation Ω are fairly accurate. The tilt τ may appear to be inaccurate, but we must be careful. Since the tilt τ is determined by neglecting the coupling with the in-plane rotation, it is only determined within errors of the magnitude of Ω. In other words, slanting followed by in-plane rotation is indistinguishable from in-plane rotation followed by slanting in the linearized theory, so that what we can best expect is $35° < \tau < 45°$. Our prediction is approximately the midpoint of that interval.

6. Concluding Remarks

Now, we summarize the merits and demerits of our scheme. A major advantage is the simplicity of the computation process per se. Once the number of intersections are counted, we can immediately compute the slant, the tilt and even the in-plane rotation by explicit formulae, and no iterative search is necessary. This is especially significant if we are dealing with moving images on line. This efficiency comes from an abstract mathematical theory and not from a simulation of human perception. We do not claim that our process is actually what happens in human brain. On the contrary, our scheme is, in a sense, superior to human perception (e.g., see Fig. 2).

The second point is memory space saving. Once the features are computed, the two-dimensional image is not necessary any more. It can be erased out of the memory. Only the computed features are to be stored. This is a profit of

feature detection in general. The third point is the 'invariance' property for motion detection. In the case of no in-plane rotations, our method is invariant to translations and dilatation-contractions, i.e., the viewer or the viewing apparatus can move right, left, up, down, forward and backward, because our second harmonics are 'invariant features' (cf. [7, 8]) with respect to these transformations. Even if the in-plane rotation is admitted, the scheme is invariant to translations. If we were to seek the correspondence of the texture and analyze its optical flow, we would face the problem of 'decoupling', i.e., we would have to separate rotational field from translational or dilatational-contractional field (cf. [23, 24]). In the present case, the decoupling is automatically incorporated in the process of feature detection.

On the other hand, there remain several problems to be solved. One of them is, of course, how to implement the scanning and the intersection counting. Physical implementation may be easy, since we only have to count the current pulses while moving a photo-cell along a prescribed line on the texture, but this is a time-consuming process. If the image is stored in memory cells, an appropriate algorithm must be devised. Although apparently there is no essential difficulty, it is out of the scope of the present paper (e.g., see [25]). Another problem arises when the entire field of view does not constitute a single plane surface moving rigidly as a whole. In this case, we must detect and cut out the portion of the image approximately in rigid motion. This process might cancel out the advantage of our process in some cases. However, if the textured surface is a flat face surrounded by a closed contour line moving against a non-textured background, detection of the moving region may be easy. In any case, thorough evaluation of the use of our method cannot be made without considering its purpose, objects observed, apparatuses used, etc. and is again out of the scope of this paper.

Finally consider the accuracy of computation. It is affected by the following factors.

(i) The spacing of parallel scanning.

(ii) The number of orientations to be scanned.

(iii) The magnitudes of high harmonics of the distribution density of the texture.

(iv) The magnitudes of the slant σ and the in-plane rotation Ω.

The spacing of parallel lines must be determined relative to the coarseness or fineness of the texture. The number of scanning orientation need not be large because we only have to compute zeroth and second harmonics. The third factor indicates that the distribution must be approximated fairly well by using only zeroth and second harmonics. In other words, the texture must not be such that it consists of line segments of only a narrow range of orientations or lacks line segments of a certain range of orientations at all. The fourth arises because ours is a linearized theory, and the slant σ and the in-plane rotation Ω must not be large, as was already mentioned.

On the other hand, since the motion of a plane is a rigid motion, the correspondence of any three different points on it would suffice to compute the motion, as is usually done in the analysis of the velocity field or the optical flow. However, this strategy is extremely sensitive to local errors, as is well known, so that we must repeat the process for a number of different sets of corresponding point pairs and take an average, or some global 'smoothness constraint' such as minimization of squared variation or Laplacian must be introduced heuristically (cf. [26]). Our scheme, on the other hand, computes in essence an average over all visible texture from the beginning and hence is 'global', as the term 'integral geometry' suggests, so that it is insensitive to local errors as long as they cancel each other after integration.

Our method is very important from a theoretical point of view because it is not heuristically devised but based on a rigorous mathematics. The basic facts we revealed are:

(i) the distribution density of line segments is obtained by intersection counting, and no curve segmentation is necessary;

(ii) the slant and tilt of a textured surface are explicitly determined by the two second Fourier coefficients of the data of intersection counting;

(iii) the relative motion of a textured surface can be detected without determining the correspondence of the texture.

At the same time, it also has a practical significance as has been pointed out so far. Meanwhile, our mathematical analysis can be used for other purposes as well. For example, we can detect the motion of a plane surface without any texture on it but surrounded by a closed contour. In this case, the surrounding contour itself can be regarded as a 'texture', and the detection is done without knowing correspondence [27, 28].

Appendix A

Note that the operation of (1) 'commutes' with rotations. Namely, put

$$\boldsymbol{B}f(\theta) = \int_0^{2\pi} |\sin(\theta - \theta')| f(\theta')\, \mathrm{d}\theta'$$

and

$$\boldsymbol{R}_\alpha f(\theta) = f(\theta - \alpha)\,,$$

i.e., $\boldsymbol{B}$ is the Buffon transform operation and $\boldsymbol{R}_\alpha$ is the rotation by α, both of which operate on the vector space $L^2(S^1)$ of functions defined on a unit circle S^1 and transform a function in it into another. Then, we can see that

$$\begin{aligned} \boldsymbol{B}\boldsymbol{R}_\alpha f(\theta) &= \int_0^{2\pi} |\sin(\theta - \theta')| f(\theta' - \alpha)\, \mathrm{d}\theta' \\ &= \int_0^{2\pi} |\sin((\theta - \alpha) - \theta')| f(\theta')\, \mathrm{d}\theta' \\ &= \boldsymbol{R}_\alpha \boldsymbol{B} f(\theta)\,, \end{aligned}$$

i.e., $\boldsymbol{B}\boldsymbol{R}_\alpha = \boldsymbol{R}_\alpha \boldsymbol{B}$ or $\boldsymbol{B} = \boldsymbol{R}_\alpha^{-1}\boldsymbol{B}\boldsymbol{R}_\alpha$. Hence, the Buffon transform operator $\boldsymbol{B}$ is an 'invariant operator' with respect to rotations and therefore must have $e^{in\theta}$ ($n = 0, \pm 1, \pm 2, \ldots$) as eigenvectors, because they span one-dimensional irreducible representations of the two-dimensional rotation group. (A formal proof of generalization to any dimensionality requires the group representation theory, especially 'Schur's lemma' and the orthogonality of irreducible representations, but in this case this is checked easily.) Since $|\sin\theta|$ is 'symmetric', i.e., $|\sin(\theta + \pi)| = |\sin\theta|$, n must be even, and since $|\sin\theta|$ is 'even', i.e., $|\sin(-\theta)| = |\sin\theta|$, $e^{in\theta}$ and $e^{-in\theta}$, or $\cos n\theta$ and $\sin n\theta$, must share the same real eigenvalue. This is a complete parallel to the 'convolution theorem' for 'time invariant' or 'stationary' linear systems and filters.

Let the nth eigenvalue be λ_n. Then, from the above group theoretical consideration, we must necessarily have

$$\int_0^{2\pi} |\sin(\theta - \phi)| \cos n\theta\, \mathrm{d}\theta = \lambda_n \cos n\phi\,,$$

$$\int_0^{2\pi} |\sin(\theta - \phi)| \sin n\theta\, \mathrm{d}\theta = \lambda_n \sin n\phi\,.$$

Since they are identities in ϕ, we can substitute any value of ϕ in these. Let $\phi = 0$. Then, we obtain from the first equation, assuming that n is an even integer,

$$\begin{aligned} \lambda_n &= \int_0^{2\pi} |\sin\theta| \cos n\theta\, \mathrm{d}\theta = 4\int_0^{\pi/2} \sin\theta \cos n\theta\, \mathrm{d}\theta \\ &= -4/(n^2 - 1)\,. \end{aligned}$$

Thus, if we expand $f(\theta)$ into Fourier series

$$f(\theta) = \frac{c}{2\pi}\left[1 + \sum_{n=2}^{\infty}{}' (a_n \cos n\theta + b_n \sin n\theta)\right], \tag{A.1}$$

$$c = \int_0^{2\pi} f(\theta)\, \mathrm{d}\theta\,, \tag{A.2}$$

$$a_n = \frac{2}{c}\int_0^{2\pi} f(\theta) \cos n\theta\, \mathrm{d}\theta, \qquad b_n = \frac{2}{c}\int_0^{2\pi} f(\theta) \sin n\theta\, \mathrm{d}\theta \tag{A.3}$$

(terms of odd n do not appear because $f(\theta)$ is symmetric), the expected number of intersections becomes

$$N(\phi) = \frac{4c}{2\pi}\left[1 - \sum_{n=2}^{\infty}{}' \frac{1}{n^2-1}(a_n \cos n\phi + b_n \sin n\phi)\right].$$

Conversely, if $N(\phi)$ is given in the form of (2), we obtain $f(\theta)$ in the form of (5).

Appendix B

Let us choose a new XY-coordinate system such that the X-axis coincides with the axis of rotation (Fig. B.1). In this coordinate system, the transformation takes the form

$$\begin{bmatrix} X' \\ Y' \end{bmatrix} = \begin{bmatrix} 1 & 0 \\ 0 & \cos\sigma \end{bmatrix} \begin{bmatrix} X \\ Y \end{bmatrix}. \tag{B.1}$$

The two coordinate systems are related by

$$\begin{bmatrix} x \\ y \end{bmatrix} = \begin{bmatrix} \cos\tau & -\sin\tau \\ \sin\tau & \cos\tau \end{bmatrix} \begin{bmatrix} X \\ Y \end{bmatrix}. \tag{B.2}$$

Hence, as is well known, the coordinate transformation of map (B.1) by (B.2) is

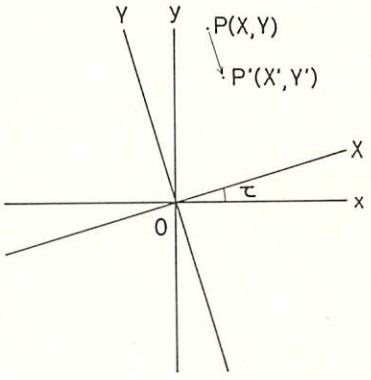

FIG. B.1. The transformation on the xy-plane induced by slant σ and tilt τ. If a new XY-coordinate system is taken so that the X-axis coincides with the axis of rotation, the transformation is viewed as shrinking by $\cos\sigma$ along the Y-axis.

given by

$$\begin{bmatrix} x' \\ y' \end{bmatrix} = \begin{bmatrix} \cos\tau & -\sin\tau \\ \sin\tau & \cos\tau \end{bmatrix} \begin{bmatrix} 1 & 0 \\ 0 & \cos\sigma \end{bmatrix} \begin{bmatrix} \cos\tau & -\sin\tau \\ \sin\tau & \cos\tau \end{bmatrix}^{-1} \begin{bmatrix} x \\ y \end{bmatrix}$$

$$= \begin{bmatrix} \cos\tau & -\sin\tau \\ \sin\tau & \cos\tau \end{bmatrix} \begin{bmatrix} 1 & 0 \\ 0 & \cos\sigma \end{bmatrix} \begin{bmatrix} \cos\tau & \sin\tau \\ -\sin\tau & \cos\tau \end{bmatrix} \begin{bmatrix} x \\ y \end{bmatrix}$$

$$= \begin{bmatrix} 1-(1-\cos\sigma)\sin^2\tau & (1-\cos\sigma)\sin\tau\cos\tau \\ (1-\cos\sigma)\sin\tau\cos\tau & 1-(1-\cos\sigma)\cos^2\tau \end{bmatrix} \begin{bmatrix} x \\ y \end{bmatrix}.$$

Appendix C

Consider Fig. C.1. Let P and Q be two nearby points on the unit circle with its center at the origin and let θ and $\theta + \mathrm{d}\theta$ be their polar angles, respectively. Suppose P and Q are mapped to P' and Q', respectively, by a linear transformation $\boldsymbol{T}$ with positive determinant (such as (9)), and let their polar angles be θ' and $\theta' + \mathrm{d}\theta'$, respectively. Draw an arc starting from P' with the center at the origin and let R be the intersection with line OQ'. Since the length of OP' is $L(\theta)$, the area of sector $P'OR$ is $\frac{1}{2}L(\theta)^2\,\mathrm{d}\theta'$. The length of OQ' is

$$L(\theta + \mathrm{d}\theta) = L(\theta) + L'(\theta)\,\mathrm{d}\theta + \mathrm{O}((\mathrm{d}\theta)^2),$$

so that the area of the remaining region $P'RQ'$ is $\frac{1}{2}L'(\theta)L(\theta)\,\mathrm{d}\theta\,\mathrm{d}\theta' + \mathrm{O}((\mathrm{d}\theta)^3)$. Thus, the area of the region $P'OQ'$ is $\frac{1}{2}L(\theta)^2\,\mathrm{d}\theta' + \mathrm{O}((\mathrm{d}\theta)^2)$. On the other hand, this region is the image of sector POQ under the linear transformation $\boldsymbol{T}$, so that its area must be $\det \boldsymbol{T}$ times the area of POQ, namely $\frac{1}{2}\det \boldsymbol{T}\,\mathrm{d}\theta$. Equating them and solving the equality for $\mathrm{d}\theta'/\mathrm{d}\theta$, we obtain (12) in the limit $\mathrm{d}\theta \to 0$.

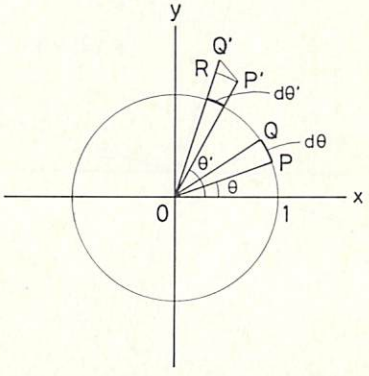

FIG. C.1. Proof of $\mathrm{d}\theta'/\mathrm{d}\theta = \det \boldsymbol{T}/L(\theta)$. Note that the area of $P'OQ'$ is $\det \boldsymbol{T}$ times that of POQ and that $OP' = L(\theta)$.

This result is easily generalized to the space of any dimensionality by the same argument. Namely, if μ is the invariant measure on the n-dimensional unit sphere S^{n-1} and $\boldsymbol{T}$ is a linear transformation of $\boldsymbol{R}^n$ with positive determinant, the Jacobian of the map induced on the sphere S^{n-1} at $\boldsymbol{n}$ (a unit vector) is given by $d\mu'/d\mu = \det \boldsymbol{T}/L(\boldsymbol{n})^n$, where $L(\boldsymbol{n})$ is defined by (10).

Appendix D

In the analysis of infinitesimal linear transformations, the Cartesian tensor calculus is most suitable because all expressions are invariant to the choice of the (Cartesian) coordinate system and the roles of the x- and y-axes are symmetric. If we use the polar coordinate system, we must resort to various 'addition theorems' of trigonometric functions to change the coordinate system and the roles of the x- and y-axes are not interchangeable, since the polar angle is measured from the x-axis.

Now, let T_{ij} be the component representation of the transformation $\boldsymbol{T}$ (with respect to an arbitrary coordinate system). In the following, we adopt the Einstein summation convention over repeated indices. First, we do not restrict $\boldsymbol{T}$ to be the form of (9) but consider all regular transformations with positive determinant. They form a group $GL^+(2, \boldsymbol{R})$ sometimes referred to as the 'deformation group', which is a Lie subgroup of $GL(2, \boldsymbol{R})$, the general linear transformation Lie group. The deformation group $GL^+(2, \boldsymbol{R})$ is the connected component of $GL(2, \boldsymbol{R})$ containing the identity. As is well known in the theory of Lie group, the connected component of a Lie group containing the identity is completely characterized by its 'Lie algebra' or 'infinitesimal transformations'.

The Lie algebra is constructed as follows. Let $\boldsymbol{T}$ be resolved into the identity transformation $\boldsymbol{I}$ and the deviation from it

$$T_{ij} = \delta_{ij} + F_{ij},$$

where δ_{ij} is the Kronecker delta. The Lie algebra is constructed by considering only linear terms in $\boldsymbol{F}$, i.e., by neglecting terms of $O(\boldsymbol{F}^2)$. The so called 'distortion tensor' $\boldsymbol{F}$ constitutes four-dimensional vector space, which is decomposed into 'invariant' (with respect to coordinate transformations) and mutually 'orthogonal' (with respect to inner product $A_{ij}B_{ij}$) subspaces. First, $\boldsymbol{F}$ is resolved into the 'symmetric part' and the 'skew part' as follows:

$$F_{ij} = e_{ij} + r_{ij},$$
$$e_{ij} \equiv F_{(ij)} \quad (= \tfrac{1}{2}(F_{ij} + F_{ji})),$$
$$r_{ij} \equiv F_{[ij]} \quad (= \tfrac{1}{2}(F_{ij} - F_{ji})).$$

Here, ( ) and [ ] designate symmetrization and antisymmetrization of indices, respectively, as indicated above. The tensors e_{ij} and r_{ij} are often referred to as the 'strain tensor' and the 'rotation tensor'. The strain tensor e_{ij} is further resolved into the 'scalar part' and the 'deviator part' as follows:

$$e_{ij} = \tfrac{1}{2}e_{kk}\delta_{ij} + \tilde{e}_{ij},$$
$$\tilde{e}_{ij} \equiv e_{\{ij\}} \quad (= e_{ij} - \tfrac{1}{2}e_{kk}\delta_{ij}).$$

Here, $\{\}$ designates the operation of taking the deviator part, i.e., making the trace zero by linearly combining its contracted components as indicated above. The scalar e_{kk} is often called the 'volumetric strain' and $\tilde{e}_{ij}$ the 'shear strain tensor'. The volumetric strain e_{kk} forms a one-dimensional subspace and the shear strain tensor $\tilde{e}_{ij}$ forms a two-dimensional subspace, while the rotation tensor r_{ij} forms a one-dimensional subspace. These three subspaces are invariant and mutually orthogonal as is easily checked, and they generate isotropic expansions (or contractions), pure shear deformations and rotations, repsectively. They form 'one-parameter subgroups' $\exp(te_{kk}\boldsymbol{I})$, $\exp(t\tilde{\boldsymbol{e}})$ and $\exp(t\boldsymbol{r})$, respectively, of $\mathrm{GL}^+(2, \boldsymbol{R})$. (Note $\exp \boldsymbol{A} \equiv \sum_{k=0}^{\infty} \boldsymbol{A}^k/k!$, which is absolutely convergent.)

Making use of these infinitesimal generators, (10)–(12) are expressed as follows:

$$L(\boldsymbol{n}) = 1 + \tfrac{1}{2}e_{kk} + \tilde{e}_{ij}n_in_j + \mathrm{O}(\boldsymbol{F}^2), \tag{D.1}$$

$$n'_i = n_i + \tilde{e}_{ij}n_j + r_{ij}n_j - \tilde{e}_{kl}n_kn_ln_i + \mathrm{O}(\boldsymbol{F}^2), \tag{D.2}$$

$$\frac{\mathrm{d}\theta'}{\mathrm{d}\theta} = 1 - 2\tilde{e}_{ij}n_in_j + \mathrm{O}(\boldsymbol{F}^2). \tag{D.3}$$

$$\det \boldsymbol{T} = 1 + e_{kk} + \mathrm{O}(\boldsymbol{F}^2). \tag{D.4}$$

In our case of (9), we obtain

$$\tilde{\boldsymbol{e}} = \frac{1-\cos\sigma}{2}\begin{bmatrix} \cos 2\tau & \sin 2\tau \\ \sin 2\tau & -\cos 2\tau \end{bmatrix}, \tag{D.5}$$

$$\mathrm{Tr}\, \boldsymbol{e} = -(1-\cos\sigma), \qquad \boldsymbol{r} = \boldsymbol{0}. \tag{D.6}$$

If we substitute (D.5) and (D.6) together with $\boldsymbol{n} = (\cos\theta, \sin\theta)^{\mathrm{T}}$ in (D.1)–(D.4) and adopt the approximation $\cos\sigma = 1 - \frac{1}{2}\sigma^2 + \frac{1}{24}\sigma^4 - \cdots$, we obtain (14)–(17). The treatment here might seem too pompous for the purpose of merely deriving (14)–(17), but the mathematical concepts introduced here plays a fundamental role in the subsequent calculation.

Appendix E

Here, we consider transformations of a Fourier series induced by infinitesimal linear transformations of the space or, to be precise, the Lie algebra of the deformation Lie group $\mathrm{GL}^+(2, \boldsymbol{R})$. Since linear transformations and their infinitesimal generators are best manipulated by the Cartesian tensor calculus, the Fourier series itself need be expressed as a (Cartesian) tensor equation invariant to coordinate transformations. This is done as follows. If we consider only even harmonics as in our present case, we can express the Fourier series in the form

$$f(\boldsymbol{n}) = \frac{c}{2\pi}\left[1 + D_{ij}n_i n_j + D_{ijkl}n_i n_j n_k n_l + \cdots\right], \tag{E.1}$$

where $D_{i_1 \cdots i_n}$ and c are computed from $f(\boldsymbol{n})$ as follows.

$$c = \int f(\boldsymbol{n})\, \mathrm{d}\mu(\boldsymbol{n}), \tag{E.2}$$

$$D_{i_1 \cdots i_n} = \frac{2^n}{c}\int n_{\{i_1} n_{i_2} \cdots n_{i_n\}} f(\boldsymbol{n})\, \mathrm{d}\mu(\boldsymbol{n}). \tag{E.3}$$

Here, $\mu(\boldsymbol{n})$ is the invariant measure on the unit circle S^1 normalized to 2π (i.e., the polar angle), and $\{\}$ designates the operator of taking the 'deviator part' of a symmetric tensor (i.e., a tensor whose value is unchanged by permutations of the indices) defined as a linear combination of various contracted components of that tensor in such a way that any contraction of it makes it zero. Specifically, if $A_{i_1 \cdots i_n}$ is a symmetric tensor, its deviator part is given by

$$\begin{aligned} A_{\{i_1 \cdots i_n\}} = {} & c_0^n A_{i_1 \cdots i_n} + c_2^n \delta_{(i_1 i_2} A_{i_3 \cdots i_n)jj} + c_4^n \delta_{(i_1 i_2}\delta_{i_3 i_4} A_{i_5 \cdots i_n)kkjj} \\ & + \cdots + c_n^n \delta_{(i_1 i_2}\delta_{i_3 i_4} \cdots \delta_{i_{n-1} i_n)} A_{j_1 j_1 j_2 j_2 \cdots j_{n/2} j_{n/2}}, \end{aligned}$$

where $()$ designates symmetrization of indices (i.e., the sum of the tensors produced by all possible permutations of its indices divided by the factorial of the number of the indices) and c_m^n are given by

$$c_m^n = \frac{(-1)^{m/2}}{2^m}\frac{n}{n - \frac{1}{2}m}\binom{n - \frac{1}{2}m}{\frac{1}{2}m}.$$

For example,

$$A_{\{ij\}} = A_{ij} - \tfrac{1}{2}\delta_{ij}A_{kk},$$

$$A_{\{ijkl\}} = A_{ijkl} - \delta_{(ij}A_{kl)mm} + \tfrac{1}{8}\delta_{(ij}\delta_{kl)}A_{mmnn}\,,$$

$$A_{\{ijklmn\}} = A_{ijklmn} - \tfrac{3}{2}\delta_{(ij}A_{klmn)pp} + \tfrac{9}{16}\delta_{(ij}\delta_{kl}A_{mn)ppqq} - \tfrac{1}{32}\delta_{(ij}\delta_{kl}\delta_{mn)}A_{ppqqrr}\,.$$

The tensor $D_{i_1\ldots i_n}$ of (E.3) is sometimes called the 'multipole moment tensor' or the 'fabric tensor', and the form (E.1) the 'multipole moment expansion'. However, expansion (E.1) is nothing but a Fourier series. Note that in our case of two dimensions each index takes either 1 or 2. Since $D_{i_1\ldots i_n}$ is a deviator tensor, it has only two distinct values. Let a_n be the value of those components whose indices have an even number of ones and b_n that of those with an odd number of ones. Then, a_n and b_n are just the Fourier coefficients (A.3) and c is the same as (A.2) in the expression (A.1).

Now, we consider transformation (13) induced by a linear map $\boldsymbol{T}$ of the space. Let the infinitesimal generators of $\boldsymbol{T}$ be defined as in Appendix D. Suppose $f(\boldsymbol{n})$ is initially given in the form

$$f(\boldsymbol{n}) = \frac{c}{2\pi}\left[1 + D_{ij}n_in_j\right]. \tag{E.4}$$

Then, by careful manipulation with the symmetries and invariances of tensors in mind, we obtain the distribution density after transformation (13) in the following form.

$$f(\boldsymbol{n}') = \frac{c'}{2\pi}\left[1 + D'_{ij}n'_in'_j + D'_{ijkl}n'_in'_jn'_kn'_l\right] + \mathrm{O}(\boldsymbol{F}^2)\,, \tag{E.5}$$

$$c' = c(1 - \tfrac{1}{2}e_{kk} + \tfrac{1}{4}\tilde{e}_{ij}D_{ij})\,, \tag{E.6}$$

$$D'_{ij} = D_{ij} + 3\tilde{e}_{ij} - \tfrac{1}{4}\tilde{e}_{kl}D_{kl}D_{ij} - 2D_{ik}r_{kj}\,, \tag{E.7}$$

$$D'_{ijkl} = -5\tilde{e}_{(ij}D_{kl)} + \tfrac{10}{3}\delta_{(ij}\tilde{e}_{k|m}D_{m|l)} - \tfrac{5}{12}\delta_{(ij}\delta_{kl)}\tilde{e}_{mn}D_{mn}\,. \tag{E.8}$$

Here, $||$ indicates exclusion from the symmetrization operation. If we apply (D.5) and (D.6) to these and use the polar angle θ, (E.4)–(E.8) reduce to (18)–(23). Perhaps, careful substitution of (14)–(17) in (18) would derive (19)–(23) and it would take just as much complication as calculation of (E.5)–(E.8). However, in deriving (E.5)–(E.8) we can always check the symmetry and invariance properties of tensor equations in the calculation process, so that tensor calculus is probably 'safer' than direct calculation in terms of the polar angle. Moreover (E.5)–(E.8) is valid for an arbitrary linear transformation, not only that of (9). Hence, this result is readily applicable when rotations or other deformations are superposed as happens in the analysis of arbitrary motion of the object (e.g., [27]).

Appendix F

The Fourier coefficients a_2 and b_2 of $f(\theta)$ are related to the Fourier coefficients A_2 and B_2 of $N(\phi)$ by $a_2 = -3A_2$ and $b_2 = -3B_2$ (cf. (2) and (5)). Hence, we also have $a_2' = -3A_2'$ and $b_2' = -3B_2'$. If we substitute these in (21) and (22), we can rearrange those equations in the matrix form

$$-\frac{3}{8}\begin{bmatrix} \frac{2}{3}-(A_2)^2 & -A_2B_2 \\ -A_2B_2 & \frac{2}{3}-(B_2)^2 \end{bmatrix}\begin{bmatrix} \sigma^2\cos 2\tau \\ \sigma^2 \sin 2\tau \end{bmatrix} = \begin{bmatrix} A_2'-A_2 \\ B_2'-B_2 \end{bmatrix},$$

which is a set of simultaneous linear equations in $\sigma^2 \cos 2\tau$ and $\sigma^2 \sin 2\tau$, giving the solution in the form

$$\begin{bmatrix} \sigma^2\cos 2\tau \\ \sigma^2 \sin 2\tau \end{bmatrix} = \frac{-4}{\frac{2}{3}-(A_2)^2-(B_2)^2}\begin{bmatrix} A \\ B \end{bmatrix}, \tag{F.1}$$

where A and B are given by (28) and (29). This is a set of two equations. If we square both sides of these two equations and add them together, we obtain

$$\sigma^4 = 16(A^2+B^2)/(\tfrac{2}{3}-(A_2)^2-(B_2)^2)^2,$$

from which results (30). If we take ratios of both sides of the equations of (F.1), we obtain

$$\tan 2\tau = B_2/A_2,$$

from which results (31).

Appendix G

The two-dimensional rotation around the origin by Ω is given by the following linear transformation

$$\boldsymbol{T} = \begin{bmatrix} \cos\Omega & \sin\Omega \\ \sin\Omega & \cos\Omega \end{bmatrix}.$$

The corresponding infinitesimal generator is given by taking the skew part

$$\boldsymbol{r} = \begin{bmatrix} 0 & \sin\Omega \\ \sin\Omega & 0 \end{bmatrix} = \begin{bmatrix} 0 & \Omega \\ \Omega & 0 \end{bmatrix} + O(\Omega^2).$$

(Note $\sin\Omega = \Omega - \frac{1}{6}\Omega^2 + \cdots$.) The Lie algebra is a vector space, so that an

additional infinitesimal transformation is just superposed linearly. In view of (E.7), the effect of this additional rotation on the Fourier coefficients is that $2\Omega b_2$ and $-2\Omega a_2$ are added to (21) and (22), respectively, while (20) is unchanged. Putting

$$c = \tfrac{1}{4}C, \qquad c' = \tfrac{1}{4}C',$$
$$a_2 = -3A_2, \quad a_2' = -3A_2',$$
$$b_2 = -3B_2, \quad b_2' = -3B_2'$$

in these equations, we obtain the following three equations.

$$C' = C[1 + \tfrac{1}{4}\sigma^2(1 - \tfrac{3}{2}(A_2 \cos 2\tau + B_2 \sin 2\tau))], \tag{G.1}$$
$$A_2' = A_2 - \sigma^2[\tfrac{1}{4}\cos 2\tau - \tfrac{3}{8}A_2(A_2 \cos 2\tau + B_2 \sin 2\tau)] - 2\Omega B_2, \tag{G.2}$$
$$B_2' = B_2 - \sigma^2[\tfrac{1}{4}\sin 2\tau - \tfrac{3}{8}B_2(A_2 \cos 2\tau + B_2 \sin 2\tau)] + 2\Omega A_2. \tag{G.3}$$

In order to solve this set of equations for σ, τ and Ω, we must realize that (G.2) and (G.3) are really a single tensor equation. Hence, we must be careful about the symmetries and invariances of tensor equations. Now, if we define angle τ_0 by (37), we have

$$A_2 \cos 2\tau + B_2 \sin 2\tau = \|\boldsymbol{A}\| \cos 2(\tau - \tau_0),$$

where the notation $\|\boldsymbol{A}\|$ is defined by (35). First, we obtain from (G.1)

$$\cos 2(\tau - \tau_0) = -\frac{8}{3}\left(\frac{C'}{C} - 1 - \tfrac{1}{4}\sigma^2\right) \Big/ \sigma^2\|\boldsymbol{A}\|. \tag{G.4}$$

Next, if we multiply (G.2) by A_2 and (G.3) by B_2 and add them together, we obtain

$$(\boldsymbol{A}, \boldsymbol{A}') = \|\boldsymbol{A}\|^2 + \|\boldsymbol{A}\|(\tfrac{3}{8}\|\boldsymbol{A}\|^2 - \tfrac{1}{4})\sigma^2 \cos 2(\tau - \tau_0),$$

where the notation $(\boldsymbol{A}, \boldsymbol{A}')$ is defined by (36). Substitution of (G.4) in this eliminates $\cos 2(\tau - \tau_0)$, and we obtain the expression for σ in the form of (32). If we substitute this form of σ back in (G.4), we obtain the expression for τ in the form of (33). On the other hand, if we multiply (G.2) by B_2 and (G.3) by A_2 and subtract the former from the latter, we obtain

$$[\boldsymbol{A}, \boldsymbol{A}'] = -\tfrac{1}{4}\sigma^2\|\boldsymbol{A}\| \sin 2(\tau - \tau_0) + 2\Omega\|\boldsymbol{A}\|^2,$$

where the notation $[\boldsymbol{A}, \boldsymbol{A}']$ is defined by (36). From this results (34).

REFERENCES

1. Marr, D.C., *Vision* (Freeman, San Francisco, CA, 1982).
2. Gibson, J.J., *The Perception of the Visual World* (Houghton Mifflin, Boston, MA, 1950).
3. Gibson, J.J., *The Senses Considered as Perceptual Systems* (Houghton Mifflin, Boston, 1966).
4. Bajcsy, R. and Lieberman, L., Texture gradients as a depth cue, *Comput. Graphics and Image Processing* **5** (1976) 52–67.
5. Stevens, K.A., The information content of texture gradients, *Biol. Cybernetics* **42** (1981) 95–105.
6. Witkin, A.P., Recovering surface shape and orientation from texture, *Artificial Intelligence* **17** (1981) 17–45.
7. Amari, S., Invariant structures of signal and feature spaces in pattern recognition problems, *RAAG Memoirs* **4** (1968) 553–566.
8. Amari, S., Feature spaces which admit and detect invariant signal transformations, *Proc. 4th Internat. Joint Conf. Pattern Recognition* (1978) 452–456.
9. Santaló, L.A., *Introduction to Integral Geometry* (Herman, Paris, 1953).
10. Kendall, M.G. and Moran, P.A., *Geometrical Probability* (Charles Griffin, London, 1963).
11. Elias, H. (Ed.), *Stereology—Proc. 2nd Internat. Congress for Stereology, Chicago, 1967* (Springer, Berlin, 1967).
12. DeHoff, R.T. and Rhines, F.N., *Quantitative Microscopy* (McGraw-Hill, New York, 1968).
13. Underwood, E.E., *Quantitative Stereology* (Addison-Wesley, Reading, MA, 1970).
14. Santaló, L.A., *Integral Geometry and Geometric Probability* (Addison-Wesley, Reading, MA, 1976).
15. Miles, R.E. and Serra, J. (Eds.), *Geometrical Probability and Biological Structures: Buffon's 200th Anniversary* (Springer, Berlin, 1978).
16. Weibel, E.R., *Stereological Methods*, Vols. 1, 2 (Academic Press, New York, 1979, 1980).
17. Ambartzumian, R.V., *Combinatorial Integral Geometry with Applications to Mathematical Stereology* (Wiley, New York, 1982).
18. Kanatani, K. and Ishikawa, O., Error analysis for the stereological estimation of sphere size distribution—Abel type integral equation, *J. Comput. Physics* (to appear).
19. Kanatani, K., Stereological determination of structural anisotropy, *Internat. J. Engrg. Sci.* **22** (1984).
20. Buffon, G., *Supplement à l'Histoire Naturalle* **4** (1777).
21. Kanatani, K., Fast Fourier transform, in: J.F. Beddow (Ed.), *Modern Methods of Fine Particle Characterization* (CRC, Boca Raton, FL, 1984).
22. Kanatani, K., Distribution of directional data and fabric tensors, *Internat. J. Engrg. Sci.* **22**(2) (1984) 149–164.
23. Longuet-Higgins, H.C. and Prazdny, K., The interpretation of a moving retinal image, *Proc. Roy. Soc. London* **B-208** (1980) 385–397.
24. Prazdny, K., Egomotion and relative depth map from optical flow, *Biol. Cybernectics* **36** (1980) 87–102.
25. Pavlidis, T., *Algorithms for Graphics and Image Processing* (Springer, Berlin, 1982).
26. Horn, B.K.P. and Schunk, B.G., Determining optical flow, *Artificial Intelligence* **17** (1981) 185–203.
27. Kanatani, K., Tracing surface motion from projection without knowing correspondence, Tech. Rept. CS-83-5, Department of Computer Science, Gunma University, 1983.
28. Kanatani, K., Detecting the motion of a planar surface by line and surface integrals, *Comput. Vision, Graphics and Image Processing* (to appear).

Received March 1983; revised version received January 1984